Robust Source Localization Exploiting Collaborative UAV Network

Shuimei Zhang, Ammar Ahmed, and Yimin D. Zhang
Department of Electrical and Computer Engineering, Temple University, Philadelphia, PA 19122, USA

***Abstract*—In this paper, we propose a robust strategy to localize multiple ground sources exploiting a distributed unmanned aerial vehicle (UAV) network in the presence of impulse noise. We achieve robust source localization by using ℓ_1-principal component analysis (ℓ_1-PCA) based signal subspace estimation at each individual UAV. This approach significantly reduces the signal subspace perturbation compared to the conventional ℓ_2-PCA based counterpart. The obtained robust signal subspace estimate is exploited to provide an improved estimate of the noise subspace, which is in turn utilized by the MUSIC algorithm to render coarse source localization at each individual UAV. The source localization information obtained at multiple UAVs is then fused by exploiting group sparsity using the re-weighted ℓ_1 minimization. Simulation results demonstrate the effectiveness of the proposed approach.**

***Index Terms*—source localization, UAV network, impulse noise, ℓ_1-norm principal component analysis, group sparsity, information fusion.**

I. Introduction

Autonomous unmanned aerial vehicles (UAVs) receive increasing attention in various civil, military, and homeland security applications, such as border surveillance, disaster monitoring, and relay communications [1]–[4]. A multi-UAV network is commonly adopted since a single UAV may not execute time-critical tasks or large-area missions due to its limited energy and payload. Multi-UAV networks also enjoy spatial diversity by sensing an area of interest from different angles, thereby significantly increasing the reliability of source localization [5]–[7].

A UAV network can perfrom real-time multi-source localization by exploiting passive sensing, localization (imaging), information transmission, and fusion. One important strategy for source localization is to utilize the angular information, which can be obtained through beamforming [8]–[12] or direction-of-arrival (DOA) estimation [13]–[22]. In particular, subspace-based DOA estimation methods have enjoyed great popularity because they achieve a high angular resolution with low computational complexity.

Conventional subspace-based DOA estimation techniques, e.g., multiple signal classification (MUSIC), achieve superior performance under the assumption of additive white Gaussian noise [15]. However, the noise often exhibits non-Gaussian properties in practice, such as low-frequency atmospheric noise and many types of man-made noise. The performance of subspace-based DOA estimation methods degrades substantially in the presence of impulsive noise, resulting in compromised source localization performance.

This work is supported in part by the National Science Foundation (NSF) under grant AST-1547420.

One common approach to mitigate the impacts of the impulse noise is to utilize the lower-order statistics to replace the second-order covariance as considered in the methods based on, e.g., the fractional lower-order moment (FLOM) [24] and the phased fractional lower-order moment (PFLOM) [25]. However, the fractional lower-order statistics based algorithms are suboptimal [23], [26]. It is noted that conventional subspace based DOA estimators rely on the ℓ_2-norm based singular value decomposition (SVD) of the data matrix and thus is highly sensitive to the outliers. Recently, an ℓ_1-norm principal component analysis (ℓ_1-PCA) based method is developed in [27]. The motivation for using the ℓ_1-norm principal components is that ℓ_1-PCA is robust to the outliers introduced by the impulsive noise [28]–[31].

Apart from the localization performance at individual UAVs, information fusion of the data obtained at multiple UAV nodes is another challenging task. One of the natural choices is to fuse the information by taking the arithmetic mean of the obtained localization images from different UAVs. However, this method does not combine the information effectively, especially when some UAVs have false positives or false negatives in the localization images. In [7] and [32], image fusion is achieved via pixel-wise multiplication. This method can suppress the sidelobes well. However, when false negatives occur at any UAV, the corresponding sources will not appear in the final fused result.

In this paper, we propose a robust source localization algorithm in the presence of impulse noise. We first exploit the ℓ_1-PCA based DOA estimation method at each UAV to obtain the coarse localization images. In this case, the effects of impulse noise are effectively mitigated by the utilization of ℓ_1-PCA MUSIC algorithm. Since the sources are sparsely located and the UAVs at different locations observe the same area of interest, the resulting localization images obtained at different UAVs are group sparse. We fuse these images by exploiting a group sparsity based approach, which utilizes re-weighted ℓ_1 minimization. It is noted that only the compressed images are transmitted among the UAV network to maintain low data traffic and network scalability.

Notations: Lower-case (upper-case) bold characters are used to denote vectors (matrices). $\boldsymbol{I}_N$ denotes the $N \times N$ identity matrix. $(\cdot)^{\mathrm{T}}$ and $(\cdot)^{\mathrm{H}}$ denote the transpose and the Hermitian transpose, respectively. Moreover, $\mathrm{diag}(\cdot)$ denotes a diagonal matrix with the elements of a vector as the diagonal entries. $\Re\{\boldsymbol{X}\}$ and $\Im\{\boldsymbol{X}\}$ denote the real and imaginary parts of $\boldsymbol{X}$, respectively. $\mathrm{E}[\cdot]$ denotes expectation. In addition, $\|\cdot\|_1$ and $\|\cdot\|_2$ express the ℓ_1 and ℓ_2 norms of a vector, respectively.

II. Problem Statement

A. Signal Model

Consider a UAV network in which each UAV is equipped with P sensors, and there are D uncorrelated far-field ground sources ($D < P$) impinging on them with respective elevation angle θ_d and azimuth angle ϕ_d, $d = 1, \cdots, D$. A spherical coordinate system is shown in Fig. 1, which describes the DOAs of the incoming plane waves. The received baseband signal vector at a UAV is modeled as:

$$\boldsymbol{x}(t) = \sum_{d=1}^{D} \boldsymbol{a}(\theta_d, \phi_d) s_d(t) + \boldsymbol{n}(t) = \boldsymbol{A}\boldsymbol{s}(t) + \boldsymbol{n}(t), \quad (1)$$

where $\boldsymbol{A} = [\boldsymbol{a}(\theta_1, \phi_1), \boldsymbol{a}(\theta_2, \phi_2), \cdots, \boldsymbol{a}(\theta_D, \phi_D)] \in \mathbb{C}^{P \times D}$ is the manifold matrix of the corresponding UAV, $\boldsymbol{s}(t) = [s_1(t), s_2(t), \cdots, s_D(t)]^{\mathrm{T}} \in \mathbb{C}^D$ is the corresponding signal vector with t denoting the discrete-time index, and $\boldsymbol{n}(t)$ is the noise vector.

In this paper, each UAV is equipped with a uniform circular array (UCA) with one element placed in the center. Compared to a uniform linear array (ULA), a UCA provides a 360° azimuthal coverage and the elevation information. The dth column of the manifold matrix $\boldsymbol{A}$ represents the steering vector of the dth source signal and is expressed as:

$$\boldsymbol{a}(\theta_d, \phi_d) = \begin{bmatrix} e^{-\jmath\zeta \sin(\theta_d)\cos(\phi_d - \beta_0)} \\ e^{-\jmath\zeta \sin(\theta_d)\cos(\phi_d - \beta_1)} \\ \vdots \\ e^{-\jmath\zeta \sin(\theta_d)\cos(\phi_d - \beta_{P-2})} \\ 1 \end{bmatrix}, \quad (2)$$

where $\zeta = 2\pi r/\lambda$, and $\beta_n = 2\pi n/(P-1)$ for $n = 0, \cdots P-2$, with r and λ respectively denoting the radius of the UCA and the wavelength of the impinging wave. Note that the central element of the UCA acts as the reference sensor.

The covariance matrix of $\boldsymbol{x}(t)$ is expressed as:

$$\boldsymbol{R}_{\boldsymbol{xx}} = \mathrm{E}\left[\boldsymbol{x}(t)\boldsymbol{x}^{\mathrm{H}}(t)\right] = \boldsymbol{A}\boldsymbol{B}\boldsymbol{A}^{\mathrm{H}} + \boldsymbol{R}_{\boldsymbol{nn}}, \quad (3)$$

where $\boldsymbol{B} = \mathrm{diag}\,[b_1, \cdots, b_D]$ is a diagonal matrix representing the power of all D sources, and $\boldsymbol{R}_{\boldsymbol{nn}}$ is the noise covariance matrix.

B. Alpha-stable Noise

If the noise follows independent and identically distributed (i.i.d.) additive white Gaussian distribution, then $\boldsymbol{R}_{\boldsymbol{nn}} = \sigma_n^2 \boldsymbol{I}_P$, where σ_n^2 denotes the noise power. On the other hand, alpha-stable distribution is commonly used to describe the impulse noise. The characteristic function of an alpha-stable random process is expressed as [33], [34]:

$$\varphi(t) = \exp\left\{j\mu t - \delta|t|^{\alpha}[1 + j\beta\,\mathrm{sgn}(t)\nu(t,\alpha)]\right\}, \quad (4)$$

where

$$\nu(t,\alpha) = \begin{cases} \tan\frac{\alpha\pi}{2}, & \alpha \neq 1, \\ \frac{2}{\pi}\log|t|, & \alpha = 1, \end{cases} \quad (5)$$

$-\infty < \mu < \infty$, $\delta > 0$, $0 < \alpha \leqslant 2$, and $-1 \leqslant \beta \leqslant 1$. Here, μ is the location parameter, δ is the dispersion parameter, α is the characteristic exponent, and β is the symmetry parameter. If $\beta = 0$, the distribution is symmetric and the observation is referred to as symmetry α-stable (SαS) distribution, which is considered in this paper.

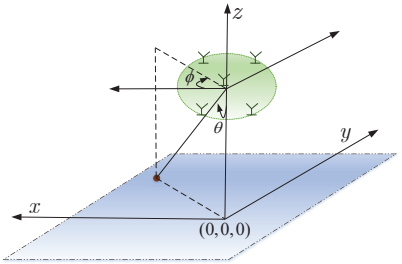

Fig. 1. The coordinate system.

C. ℓ_2-PCA Based MUSIC

In practice, the actual covariance matrix $\boldsymbol{R}_{\boldsymbol{xx}}$ is usually unavailable and is estimated from the data samples as:

$$\hat{\boldsymbol{R}}_{\boldsymbol{xx}} = \frac{1}{K}\sum_{t=1}^{K} \boldsymbol{x}(t)\boldsymbol{x}^{\mathrm{H}}(t) = \frac{1}{K}\boldsymbol{X}\boldsymbol{X}^{\mathrm{H}}, \quad (6)$$

where $\boldsymbol{X} = [\boldsymbol{x}(1), \cdots, \boldsymbol{x}(K)] \in \mathbb{C}^{P \times K}$ is the received data matrix consisting of K snapshots.

The signal subspace consists of the D-dimensional principal subspace of $\hat{\boldsymbol{R}}_{\boldsymbol{xx}}$, which is spanned by the eigenvectors associated with the D highest eigenvalues. In fact, the solution of the following ℓ_2-PCA problem results in the eigenvectors of $\hat{\boldsymbol{R}}_{\boldsymbol{xx}}$ or the left singular vectors of $\boldsymbol{X}$ [27]:

$$\boldsymbol{U}_{\ell_2}^{s} = \underset{\boldsymbol{U} \in \mathbb{C}^{P \times D}, \boldsymbol{U}^{\mathrm{H}}\boldsymbol{U} = \boldsymbol{I}_D}{\arg\max} \|\boldsymbol{U}^{\mathrm{H}}\boldsymbol{X}\|_2^2. \quad (7)$$

The noise subspace spanned by $\boldsymbol{U}_{\ell_2}^{n}$ is orthogonal to the signal subspace spanned by $\boldsymbol{U}_{\ell_2}^{s}$, i.e.,

$$\boldsymbol{U}_{\ell_2}^{n}(\boldsymbol{U}_{\ell_2}^{n})^{\mathrm{H}} = \boldsymbol{I}_P - \boldsymbol{U}_{\ell_2}^{s}(\boldsymbol{U}_{\ell_2}^{s})^{\mathrm{H}}. \quad (8)$$

The conventional MUSIC algorithm is based on the ℓ_2-PCA and computes the following spatial pseudo-spectrum:

$$p_{\ell_2}(\theta_d, \phi_d) = \frac{1}{\boldsymbol{a}^{\mathrm{H}}(\theta_d, \phi_d)\boldsymbol{U}_{\ell_2}^{n}(\boldsymbol{U}_{\ell_2}^{n})^{\mathrm{H}}\boldsymbol{a}(\theta_d, \phi_d)}. \quad (9)$$

MUSIC detects the D sources from the local peaks of Eq. (9). Under SαS noise, however, the signal subspace obtained from (7) is inaccurate, thus resulting in severe performance degradation of the conventional MUSIC algorithm.

III. Proposed Method

In this section, we describe a collaborative robust source localization algorithm for UAV networks. First, we apply an ℓ_1-PCA based MUSIC technique on the sampled data acquired at each UAV node to obtain the coarse images of the ground sources in the presence of SαS noise. Subsequently, each UAV compresses its estimated localization image by using singular value decomposition (SVD) and then wirelessly transfers it to the master UAV node. The master node, which acts as the fusion center, fuses the localization images by exploiting group sparse reconstruction based on re-weighted ℓ_1 minimization.

A. Image Formation via ℓ_1-PCA Based MUSIC

The ℓ_1-norm tends to maintain sturdy resistance against outliers when the received data is corrupted. Instead of ℓ_2-norm maximization, ℓ_1-norm maximization can be exploited in problem (7), and the corresponding ℓ_1-PCA problem can be expressed as:

$$\boldsymbol{U}_{\ell_1}^{s} = \underset{\boldsymbol{U}\in\mathbb{C}^{P\times D},\boldsymbol{U}^{\mathrm{H}}\boldsymbol{U}=\boldsymbol{I}_D}{\arg\max} \|\boldsymbol{U}^{\mathrm{H}}\boldsymbol{X}\|_1. \tag{10}$$

Given the fact that ℓ_1-PCA is developed originally for the real-valued data, the complex-number realification is utilized to recast our complex data into a real-data problem as [27]

$$\overline{\boldsymbol{X}} \triangleq \begin{bmatrix} \Re\{\boldsymbol{X}\}, & -\Im\{\boldsymbol{X}\} \\ \Im\{\boldsymbol{X}\}, & \Re\{\boldsymbol{X}\} \end{bmatrix} \in \mathbb{R}^{2P\times 2K}, \tag{11}$$

where $\overline{(\cdot)}$ denotes the complex realification. In this case, (10) can be reformulated as:

$$\overline{\boldsymbol{U}}_{\ell_1}^{s} = \underset{\overline{\boldsymbol{U}}\in\mathbb{R}^{2P\times 2D},\overline{\boldsymbol{U}}^{\mathrm{H}}\overline{\boldsymbol{U}}=\boldsymbol{I}_{2D}}{\arg\max} \|\overline{\boldsymbol{U}}^{\mathrm{H}}\overline{\boldsymbol{X}}\|_1. \tag{12}$$

Denote $\overline{\boldsymbol{R}}_{\ell_1} = \overline{\boldsymbol{U}}_{\ell_1}^{s}(\overline{\boldsymbol{U}}_{\ell_1}^{s})^{\mathrm{T}} \in \mathbb{R}^{2P\times 2P}$. The signal subspace is expressed as:

$$\boldsymbol{R}_{\ell_1}^{s} = \overline{\boldsymbol{R}}_{\ell_1}[1\colon P, 1\colon P] + \jmath\overline{\boldsymbol{R}}_{\ell_1}[P+1\colon 2P, 1\colon P] \in \mathbb{C}^{P\times P}, \tag{13}$$

where $\boldsymbol{A}[h\colon i, j\colon k]$ represents a sub-matrix of $\boldsymbol{A}$ which consists of the elements from the hth row and the jth column to the ith row and the kth column. The noise subspace is obtained as:

$$\boldsymbol{R}_{\ell_1}^{n} = \boldsymbol{I}_P - \boldsymbol{R}_{\ell_1}^{s}. \tag{14}$$

Consider a two-dimensional $L \times L$ source scene in the observation area, where $M = L \times L \gg D$ is the total number of pixels. The value of the spatial pseudo-spectrum at the mth pixel is the output from the ℓ_1-PCA based MUSIC estimator, given by

$$p_{\ell_1}(\theta_m, \phi_m) = \frac{1}{\boldsymbol{a}^{\mathrm{H}}(\theta_m, \phi_m)\boldsymbol{R}_{\ell_1}^{n}\boldsymbol{a}(\theta_m, \phi_m)}, \tag{15}$$

for $m = 1, \cdots, M$. Repeating Eq. (15) pixel by pixel, we obtain the ℓ_1-PCA based MUSIC image $\boldsymbol{I}_g$ of the gth UAV for $g = 1, \cdots, G$.

B. Image Fusion via Enhanced Group-Sparsity

All images $\boldsymbol{I}_g, g = 1, \cdots, G$, obtained from the ℓ_1-PCA based MUSIC technique are transmitted to the fusion center in a compressed form [37]. Since the images obtained at different UAVs correspond to the same sparse scene of the sources, they exhibit group sparsity which helps obtain the correct sparsity support and suppress undesired sporadic results [35].

Define $\boldsymbol{i}_g = \mathrm{vec}(\boldsymbol{I}_g)$, where $\mathrm{vec}(\cdot)$ denotes the matrix vectorization. The group sparsity is employed as:

$$\begin{aligned} \min_{\boldsymbol{w}_g} \quad & \sum_{g=1}^{G} \|\boldsymbol{i}_g - \boldsymbol{\Phi}\boldsymbol{w}_g\|_2^2 \\ \text{subject to} \quad & \sum_{m=1}^{M}\left(\sum_{g=1}^{G}|w_{g,m}|^2\right)^{1/2} \le \gamma_{\mathrm{tol}}, \end{aligned} \tag{16}$$

where γ_{tol} is the acceptable tolerance, $\boldsymbol{\Phi} \in \mathbb{R}^{M\times M}$ is the dictionary matrix which, in the underlying application, is an identity matrix, and $w_{g,m}$ denotes the mth element of the vector $\boldsymbol{w}_g \in \mathbb{R}^M$ for the gth UAV which serves as the vectorized form of the fused final estimates. The optimization (16) can be reformulated as follows:

$$\hat{\boldsymbol{w}}_g = \min_{\boldsymbol{w}_g} \sum_{g=1}^{G} \|\boldsymbol{i}_g - \boldsymbol{\Phi}\boldsymbol{w}_g\|_2^2 + \eta \sum_{m=1}^{M}\left(\sum_{g=1}^{G}|w_{g,m}|^2\right)^{1/2}, \tag{17}$$

where η is the regularization parameter.

When the sources are observed with different strengths, the group sparse reconstruction can be enhanced by utilizing the following weighting function [36]:

$$v_m^{(n)} = \begin{cases} \left(\sum_{g=1}^{G}|\hat{w}_{g,m}^{(n-1)}|^2\right)^{-1/2}, & \text{if } \sum_{g=1}^{G}|\hat{w}_{g,m}^{(n-1)}|^2 > 0, \\ 1/\epsilon, & \text{if } \sum_{g=1}^{G}|\hat{w}_{g,m}^{(n-1)}|^2 = 0, \end{cases} \tag{18}$$

where $v_m^{(n)}$ denotes the weighting coefficient for the nth iteration, and ϵ should ideally be slightly less than the minimum non-zero value of $\boldsymbol{w}_g$. Large weights are used to discourage nonzero entries, while small weights are used to encourage nonzero entries. It results in the following re-weighted ℓ_1-minimization group sparse reconstruction problem:

$$\hat{\boldsymbol{w}}_g^{(\mathrm{n})} = \min_{\boldsymbol{w}_g} \sum_{g=1}^{G} \|\boldsymbol{i}_g - \boldsymbol{\Phi}\boldsymbol{w}_g\|_2^2 + \eta \sum_{m=1}^{M} v_m^{(n)}\left(\sum_{g=1}^{G}|w_{g,m}|^2\right)^{1/2}. \tag{19}$$

We solve (19) in an iterative fashion until convergence. The final fused image can be computed as follows:

$$\hat{\mathbf{W}} = \mathrm{ivec}\left(\hat{\boldsymbol{w}}\right) = \mathrm{ivec}\left(\sum_{g=1}^{G}|\hat{\boldsymbol{w}}_g|\right), \tag{20}$$

where $\mathrm{ivec}(\cdot)$ denotes the inverse of vectorization operation.

IV. Simulation Results

In this section, we provide simulation results to demonstrate the performance of the proposed robust source localization method. Five UAVs are considered with their respective locations at $(-80, 0, 120)$ m, $(-40, 69, 120)$ m, $(0, 5, 120)$ m, $(40, 69, 120)$ m, and $(80, 0, 120)$ m. Each UAV is equipped

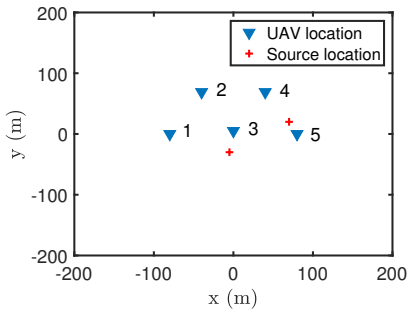

Fig. 2. The UAV network configuration.

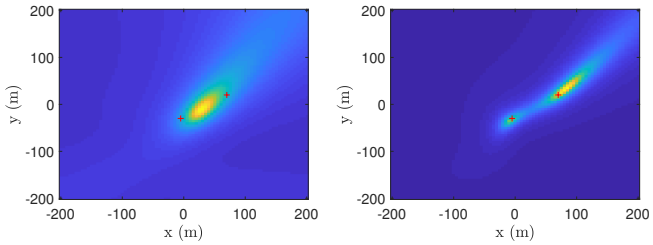

(a) ℓ_2-PCA based for UAV 1

(b) ℓ_1-PCA based for UAV 1

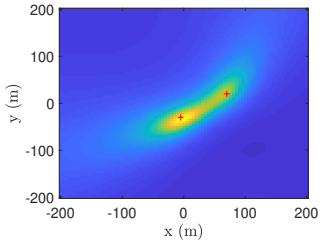

(c) ℓ_2-PCA based for UAV 2

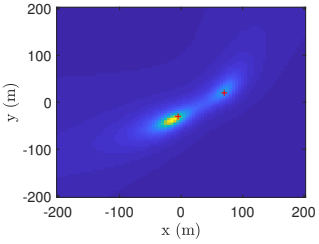

(d) ℓ_1-PCA based for UAV 2

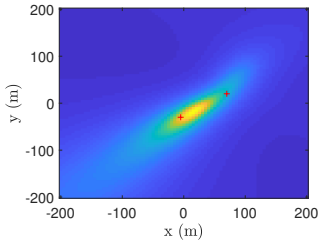

(e) ℓ_2-PCA based for UAV 3

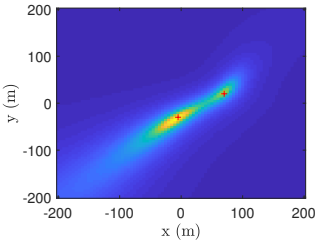

(f) ℓ_1-PCA based for UAV 3

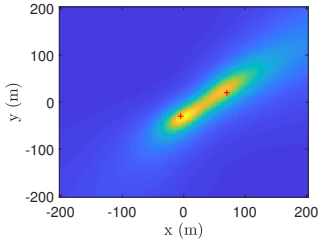

(g) ℓ_2-PCA based for UAV 4

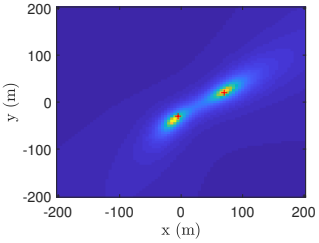

(h) ℓ_1-PCA based for UAV 4

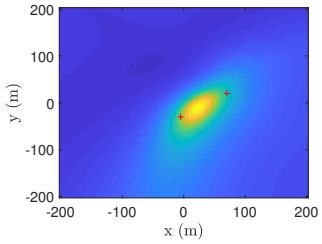

(i) ℓ_2-PCA based for UAV 5

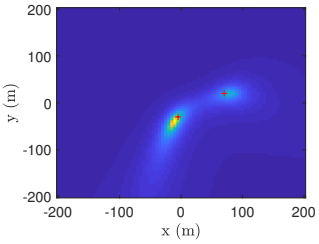

(j) ℓ_1-PCA based for UAV 5

Fig. 3. Comparison of conventional ℓ_2-PCA based MUSIC (first column) and ℓ_1-PCA based MUSIC (second column) under $S\alpha S$ noise.

with a UCA consisting of 5 elements. The simulations focus on a small search area with a size of $400\,\text{m} \times 400\,\text{m}$ on the ground. As shown in Fig. 2, there are two ground sources located at $(-5, -30, 0)$ m and $(70, 20, 0)$ m, respectively. The grid interval is chosen to be 5 m. Moreover, the third UAV is chosen as the fusion center. To reduce the traffic during information

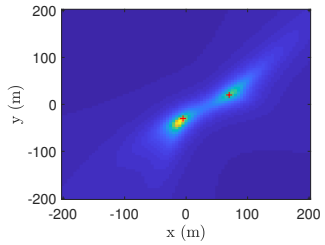

(a) Arithmetic averaging

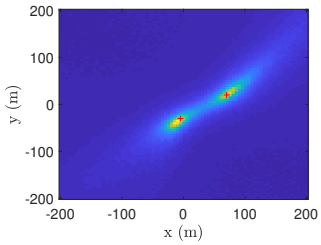

(b) Group sparsity (proposed)

Fig. 4. Comparison of the fused images.

transmission, the localization images are compressed via SVD [37] and are then decompressed at the fusion center.

We consider $S\alpha S$ impulsive noise and the generalized SNR (GSNR), defined as $10\log(\text{E}[|s(t)|^2]/\gamma)$, is set to 7 dB in all simulations, where $\gamma = 0.2$ and $\alpha = 1.5$. Matlab codes available at [38] and [39] are used to compute $S\alpha S$ distribution noise and ℓ_1-PCA, respectively. For fair comparison, the maximum values of all plots in Figs. 3 and 4 are normalized to unity. The color bar is set to $[0, 1]$ for all plots.

In Fig. 3, the first column presents the ℓ_2-PCA based MUSIC images from each UAV whereas the second column presents the counterparts using the ℓ_1-PCA based MUSIC. Each row in Fig. 3 corresponds to a single UAV. It is observed that, for the ℓ_2-PCA based MUSIC method, none of the UAVs clearly resolves the two sources.

In comparison, the imaging results shown in the second column of Fig. 3 are obtained by exploiting the ℓ_1-PCA based MUSIC algorithm. It can be observed that the ℓ_1-PCA based strategy effectively mitigates the effects of outliers caused by the impulse noise and subsequently yields successful source resolution and localization at each UAV.

It is noticed in Fig. 3 that the localization images obtained at individual UAVs vary in their quality and shapes around the true source positions, thus motivating effective fusion of these images into an improved solution. The fused image obtained by taking a simple arithmetic mean of the ℓ_2-PCA based MUSIC images from the five UAVs as shown in the first column of Fig. 3 is presented in Fig. 4(a). It is observed that the two sources are resolved, but with noticeable bias and incorrect signal levels. On the other hand, Fig. 4(b) shows the result of the proposed method, which fuses the ℓ_1-PCA based MUSIC images by exploiting group sparse reconstruction. The proposed fusion method represents the two sources much more clearly and accurately illustrates their signal levels.

V. Conclusion

In this paper, we proposed a robust source localization technique in the presence of impulse noise. The ℓ_1-PCA based MUSIC technique is individually performed at each UAV to robustly obtain the initial localization images, whereas the re-weighted group-sparsity based image fusion method is performed to obtain the final localization image at the fusion center. Simulation results verified the effectiveness of the proposed strategy.

REFERENCES

[1] A. Ryan, M. Zennaro, A. Howell, R. Sengupta, and J. Hedrick, "An overview of emerging results in cooperative UAV control," in *Proc. IEEE Conf. Decision and Control*, Nassau, Bahamas, Dec. 2004, pp. 602–607.

[2] D. Cole, A. Goktogan, P. Thompson, and S. Sukkarieh, "Mapping and tracking," *IEEE Robot. Autom. Mag.*, vol. 16, pp. 22–34, June 2009.

[3] X. Li and Y. D. Zhang, "Multi-source cooperative communications using multiple small relay UAVs," in *Proc. IEEE Globecom Workshop on Wireless Networking for Unmanned Aerial Vehicles*, Miami, FL, Dec. 2010, pp. 1805–1810.

[4] B. K. Chalise, Y. D. Zhang, and M. G. Amin, "Multi-beam scheduling for unmanned aerial vehicle networks," in *Proc. IEEE/CIC Int. Conf. Commun.*, Xi'an, China, Aug. 2013, pp. 442–447.

[5] M. Mozaffari, W. Saad, M. Bennis, Y-H. Namm and M. Debbah, "A tutorial on UAVs for wireless networks: Applications, challenges, and open problems," *IEEE Commun. Surveys & Tutorials*, vol. 21, pp. 2334–2360, 3rd Quarter 2019.

[6] A. Ahmed, S. Zhang, and Y. D. Zhang, "Multi-target motion parameter estimation exploiting collaborative UAV network," in *Proc. IEEE Int. Conf. Acoust. Speech Signal Process.*, Brighton, U.K., May 2019, pp. 4459–4463.

[7] S. Zhang, A. Ahmed, and Y. D. Zhang, "Sparsity-based collaborative sensing in a scalable wireless network," in *Proc. SPIE Big Data: Learning, Analytics, and Applications*, vol. 10989, Baltimore, MD, May 2019.

[8] H. L. Van Trees, *Optimum Array Processing: Part IV of Detection, Estimation, and Modulation Theory*. Wiley, 2002.

[9] S. Zhang, Y. Gu, B. Wang, and Y. D. Zhang, "Robust astronomical imaging under coexistence with wireless communications," in *Proc. Asilomar Conf. Signals, Systems, and Computers*, Pacific Grove, CA, Nov. 2017.

[10] K. Liu and Y. D. Zhang, "Coprime array-based robust beamforming using covariance matrix reconstruction technique," *IET Commun.*, vol. 12, pp. 2206–2212, Oct. 2018.

[11] S. Zhang, Y. Gu, and Y. D. Zhang, "Robust astronomical imaging in the presence of radio frequency interference," *J. Astronom. Instrument.*, vol. 8, ID 1940012, pp. 1–15, 2019.

[12] Y. Gu, N. A. Goodman, and Y. D. Zhang, "Adaptive beamforming via sparsity-based reconstruction of covariance matrix," in A. De Maio, Y. C. Eldar, and A. Haimovich (eds.), *Compressed Sensing in Radar Signal Processing*, Cambridge Univ. Press, 2019.

[13] R. O. Schmidt, "Multiple emitter location and signal parameter estimation," *IEEE Trans. Antennas Propag.*, vol. 34, pp. 276–280, 1986.

[14] I. Ziskind and M. Wax, "Maximum likelihood localization of multiple sources by alternating projection," *IEEE Trans. Acoust., Speech, Signal Process.,* vol. 36, pp. 1553–1560, Oct. 1988.

[15] P. Stoica and A. Nehorai, "MUSIC, maximum likelihood, and Cramer-Rao bound," *IEEE Trans. Acoustics, Speech, Signal Process.*, vol. 37, pp. 720–741, May 1989.

[16] H. Krim and M. Viberg, "Two decades of array signal processing research: the parametric approach," *IEEE Signal Process. Mag.*, vol. 13, pp. 67–94, July 1996.

[17] T. E. Tuncer and B. Friedlander, *Classical and Modern Direction-of-Arrival Estimation*. Elsevier, 2009.

[18] S. Qin, Y. D. Zhang, and M. G. Amin, "Generalized coprime array configurations for direction-of-arrival estimation," *IEEE Trans. Signal Process.*, vol. 63, pp. 1377–1390, March 2015.

[19] B. Wang, Y. D. Zhang, and W. Wang, "Robust DOA estimation in the presence of miscalibrated sensors," *IEEE Signal Process. Lett.*, vol. 24, pp. 1073–1077, July 2017.

[20] A. Ahmed, Y. D. Zhang, and B. Himed, "Effective nested array design for fourth-order cumulant-based DOA estimation," in *Proc. IEEE Radar Conf.*, Seattle, WA, May 2017, pp. 998–1002.

[21] M. Guo, Y. D. Zhang, and T. Chen, "DOA estimation using compressed sparse array," *IEEE Trans. Signal Process.*, vol. 66, pp. 4133–4146, Aug. 2018.

[22] A. Ahmed, Y. D. Zhang, and J-K. Zhang, "Coprime array design with minimum lag redundancy," in *Proc. IEEE Int. Conf. Acoust., Speech, Signal Process.*, Brighton, U.K., May 2019.

[23] F. Pascal, P. Forster, J-P. Ovarlez, and P. Larzabal, "Performance analysis of covariance matrix estimates in impulsive noise," *IEEE Trans. Signal Process.*, vol. 56, pp. 2206–2217, June 2008.

[24] T.-H. Liu and J. M. Mendel, "A subspace-based direction finding algorithm using fractional lower order statistics," *IEEE Trans. Signal Process.*, vol. 49, pp. 1605–1613, Aug. 2001.

[25] H. Belkacemi and S. Marcos, "Robust subspace-based algorithms for joint angle/doppler estimation in non-Gaussian clutter," *Signal Process.*, vol. 87, pp. 1547–1558, Jan. 2007.

[26] R. J. Kozick and B. M. Sadler, "Maximum-likelihood array processing in non-Gaussian noise with Gaussian mixtures," *IEEE Trans. Signal Process.*, vol. 48, pp. 3520–3535, Dec. 2000.

[27] P. P. Markopoulos, N. Tsagkarakis, D. A. Pados and G. N. Karystinos, "Realified l1-PCA for direction-of-arrival estimation: theory and algorithms," *EURASIP J. Adv. Signal Process.*, vol. 2019, ID 30, pp. 1-16, 2019.

[28] P. P. Markopoulos, G. N. Karystinos, and D. A. Pados, "Optimal algorithms for l1-subspace signal processing," *IEEE Trans. Signal Process.*, vol. 62, pp. 5046–5058, Oct. 2014.

[29] P. P. Markopoulos, S. Kundu, S. Chamadia, and D. A. Pados, "Efficient l1-norm principal-component analysis via bit flipping," *IEEE Trans. Signal Process.*, vol. 65, pp. 4252–4264, Aug. 2017.

[30] P. P. Markopoulos, M. Dhanaraj, and A. Savakis, "Adaptive l1-norm principal-component analysis with online outlier rejection," *IEEE J. Sel. Top. Signal Process.*, vol. 12, pp. 1131–1143, Dec. 2018.

[31] N. Tsagkarakis, P. P. Markopoulos, G. Sklivanitis, and D. A. Pados, "L1-norm principal component analysis of complex data," *IEEE Trans. Signal Process.*, vol. 66, pp. 3256–3267, Mar. 2018.

[32] D. Comite, F. Ahmad, D. Liao, T. Dogaru, and M. G. Amin, "Multiview imaging for low-signature target detection in rough-surface clutter environment," *IEEE Trans. Geosci. Remote Sens.*, vol. 55, pp. 5220–5229, Sept. 2017.

[33] D. Middleton, "Non-Gaussian noise models in signal processing for telecommunications: New methods and results for class A and class B noise models," *IEEE Trans. Inf. Theory*, vol. 45, pp. 1129–1149, May 1999.

[34] D. Zha and T. Qiu, "Direction finding in non-Gaussian impulsive noise environments," *Digital Signal Process.*, vol. 17, pp. 451–465, 2007.

[35] S. Subedi, Y. D. Zhang, M. G. Amin, and B. Himed, "Group sparsity based multi-target tracking in passive multi-static radar systems using Doppler-only measurements," *IEEE Trans. Signal Process.*, vol. 64, pp. 3619–3634, July 2016.

[36] E. J. Candés, M. B. Wakin, and S. P. Boyd, "Enhancing sparsity by reweighted ℓ-1 minimization," *J. Fourier Anal. Appl.*, vol. 14, pp. 877–905, Dec. 2008.

[37] H. S. Prasantha, H. L. Shashidhara, and K. N. B. Murthy, "Image compression using SVD," in *Proc. Int. Conf. Comput. Intell. Multimedia Appl.*, vol. 3, Tamil Nadu, India, Dec. 2007, pp. 143–145.

[38] M. Veillette, "Alpha-stable distributions in MATLAB," http://math.bu.edu/people/mveillet/html/alphastablepub.html

[39] P. P. Markopoulos, "L1-PCA toolbox," https://www.mathworks.com/matlabcentral/fileexchange/64855-l1-PCA-toolbox